








Association between Texture Analysis Parameters and Molecular Biologic KRAS Mutation in Non-Mucinous Rectal Cancer

원발성 비점액성 직장암 환자에서 자기공명영상 기반 텍스처 분석 변수와 KRAS 유전자 변이와의 연관성

Sung Jae Jo, MD¹ , Seung Ho Kim, MD^{1*} , Sang Joon Park, PhD² ,
Yedaun Lee, MD¹ , Jung Hee Son, MD¹ 

¹Department of Radiology, Inje University College of Medicine, Haeundae Paik Hospital, Busan, Korea

²Department of Radiology, Seoul National University Hospital, Seoul, Korea

Purpose To evaluate the association between magnetic resonance imaging (MRI)-based texture parameters and Kirsten rat sarcoma viral oncogene homolog (KRAS) mutation in patients with non-mucinous rectal cancer.

Materials and Methods Seventy-nine patients who had pathologically confirmed rectal non-mucinous adenocarcinoma with or without KRAS-mutation and had undergone rectal MRI were divided into a training ($n = 46$) and validation dataset ($n = 33$). A texture analysis was performed on the axial T2-weighted images. The association was statistically analyzed using the Mann-Whitney U test. To extract an optimal cut-off value for the prediction of KRAS mutation, a receiver operating characteristic curve analysis was performed. The cut-off value was verified using the validation dataset.

Results In the training dataset, skewness in the mutant group ($n = 22$) was significantly higher than in the wild-type group ($n = 24$) (0.221 ± 0.283 ; -0.006 ± 0.178 , respectively, $p = 0.003$). The area under the curve of the skewness was 0.757 (95% confidence interval, 0.606 to 0.872) with a maximum accuracy of 71%, a sensitivity of 64%, and a specificity of 78%. None of the other texture parameters were associated with KRAS mutation ($p > 0.05$). When a cut-off value of 0.078 was applied to the validation dataset, this had an accuracy of 76%, a sensitivity of 86%, and a specificity of 68%.

Conclusion Skewness was associated with KRAS mutation in patients with non-mucinous rectal cancer.

Index terms Magnetic Resonance Imaging; Rectum; Neoplasm; Computer; Software; Oncogene

Received April 6, 2020

Revised June 3, 2020

Accepted June 23, 2020

*Corresponding author

Seung Ho Kim, MD
Department of Radiology,
Inje University College of Medicine,
Haeundae Paik Hospital,
875 Haeun-daero, Haeundae-gu,
Busan 48108, Korea.

Tel 82-51-797-0382

Fax 82-51-797-0379

E-mail radiresi@gmail.com

This is an Open Access article distributed under the terms of the Creative Commons Attribution Non-Commercial License (<https://creativecommons.org/licenses/by-nc/4.0>) which permits unrestricted non-commercial use, distribution, and reproduction in any medium, provided the original work is properly cited.

ORCID iDs

Sung Jae Jo 
[https://
orcid.org/0000-0001-8190-7744](https://orcid.org/0000-0001-8190-7744)
Seung Ho Kim 
[https://
orcid.org/0000-0002-9402-9642](https://orcid.org/0000-0002-9402-9642)
Sang Joon Park 
[https://
orcid.org/0000-0003-1013-681X](https://orcid.org/0000-0003-1013-681X)
Yedaun Lee 
[https://
orcid.org/0000-0002-9801-8449](https://orcid.org/0000-0002-9801-8449)
Jung Hee Son 
[https://
orcid.org/0000-0002-9557-5848](https://orcid.org/0000-0002-9557-5848)

INTRODUCTION

Texture analysis refers to a class of mathematical procedures and models that characterize spatial variations within imagery as a means of extracting information (1). Structural, statistical, model-based and transform-based approaches are representative methods of texture analysis (2). Statistical approaches, which have been most widely used, analyze the spatial distributions and relationships among the gray-level values of an image (1, 2). Statistical methods are further divided into first-order, second-order, and higher-order statistics. First-order statistics measure the properties of individual pixel values, and the statistical parameters are mean, variance, standard deviation (SD), skewness, kurtosis, entropy and homogeneity (1, 3, 4). Second-order statistics measure the properties of two or more pixel values. The gray-level co-occurrence matrix (GLCM), defined as a two-dimensional (2D) histogram of gray levels for a pair of pixels that are separated according to a fixed spatial relationship, is the most commonly used method for measuring texture properties and extracting texture features (1, 5). The relevant parameters are moment, angular second moment (ASM), inverse difference moment (IDM), contrast, and entropy (3, 5). The definitions of the texture features are summarized in Table 1.

Texture analysis has recently been used as a quantitative imaging tool in oncologic studies and is becoming increasingly common (4). Several studies applied texture analysis of magnetic resonance imaging (MRI) as an imaging biomarker for assessment of tumor staging, treatment response, prognosis, and survival in patients with colorectal cancer (CRC) (6-15).

Molecular biologically, Kirsten rat sarcoma viral oncogene homolog (KRAS) mutation has been proven to be a predictive biomarker of resistance to anti-epidermal growth factor receptor (EGFR) therapy (16). Specifically, it is well known that KRAS mutation is associated with poor response to anti-EGFR therapy (17, 18). MRI is widely used to determine clinical staging and treatment planning in rectal cancer (19, 20). However, there is as yet no imaging approach that can predict KRAS mutation without relying on molecular biologic confirma-

Table 1. Definitions of Texture Parameters

Texture Parameters	Definition
First-order texture features	
Mean	Average of pixel value
Standard deviation	Variation from mean gray-level value
Skewness	Measure of histogram symmetry
Kurtosis	Measure of histogram flatness
Entropy	Measure of irregularity of gray-level distribution
Homogeneity	Measure of homogeneity of gray-level distribution
Second-order texture features (GLCM based)	
ASM	Measure of textural uniformity in image
IDM	Measure of homogeneity in image
Contrast	Measure of spatial frequency in image
Entropy	Measure of disorder or complexity in image

ASM = angular second moment, GLCM = gray-level co-occurrence matrix, IDM = inverse difference moment

tion. Moreover, to the best of our knowledge, there are only a few studies that have assessed the association between MRI-based texture analysis-derived parameters and KRAS mutation in rectal cancer (21). Therefore, the aim of this study was to investigate the association between them in patients with non-mucinous rectal cancer.

MATERIALS AND METHODS

This retrospective study was approved by the relevant Institutional Review Board, and informed consent was waived (IRB No. 2019-02-022-001).

PATIENTS AND SELECTION CRITERIA

Between September 2014 and December 2018, a total of 390 patients were surgically and histologically revealed to have rectal adenocarcinoma. Among them, 79 patients who met the inclusion criteria were included in the training dataset. The inclusion criteria were as follows: 1) rectal MRI performed prior to treatment and 2) data on KRAS-mutation status. Out of the 79 patients, 33 patients were excluded due to the following reasons: 1) neoadjuvant chemo-radiation therapy prior to surgery ($n = 22$) and 2) histopathologic diagnosis of mucinous subtype ($n = 11$). A total of 46 patients (male: 35, female: 11, mean age: 64 years, range: 48-87 years) were enrolled in the training dataset.

For a validation dataset, 35 consecutive patients who satisfied the same inclusion criteria between January 2019 and March 2020 were recruited. Patients with mucinous subtype ($n = 2$) were also excluded. The validation dataset consisted of 33 patients (male: 25, female: 8, mean age: 63 years, range: 40-84 years).

MR IMAGING

All rectal MRI was obtained with a 3.0-T MR machine (Achieva; Philips Medical Imaging, Best, the Netherlands) with a phased-array body coil (Torso-pelvis coil; USA Instruments, Aurora, OH, USA).

The imaging protocol included axial, coronal and sagittal T2-weighted turbo spin-echo (T2WI) sequences (repetition time/echo time, 3727/90 msec; echo train length, 17; slice thickness, 3 mm; slice gap, 0.3 mm; matrix size, 300×290 ; number of excitations, 1; field of view, 240×240). The longest tumor axis was identified on sagittal T2WI, and axial and coronal T2WI were acquired perpendicularly and parallel to the longest tumor axis, respectively.

MR TEXTURE ANALYSIS

Prior to performing the texture analysis, two radiologists with 15 and 3 years of experience in rectal MRI, respectively, reviewed the T2WI in three planes, and determined the location and border of each tumor by consensus. Both radiologists were blinded to the presence of KRAS mutation.

The MR DICOM images of axial T2WI were transferred from a picture archiving and communication system (PACS) workstation (m-view; Marotech, Seoul, Korea) to a workstation equipped with in-house software (Medical Imaging Solution for Segmentation and Texture Analysis, MISSTA, Seoul, Korea) that performs fully automated quantification of texture fea-

tures implemented using a dedicated C++ language (Microsoft Foundation Classes; Microsoft, Redmond, WA, USA) (22-26). The radiologist with 3 years of experience manually drew regions of interest (ROIs) around the tumor border in each section of axial T2WI to cover the entire tumor volume using the 3D measurement tool of the software. Definite areas of necrosis, hemorrhage, fat, vessel or bowel were excluded from the ROIs. After the tumor segmentation, the texture features (i.e., histogram parameters, volumetric parameters, morphologic parameters) were automatically calculated by the texture analysis software. The texture features included statistical first-order statistics (mean, variance, SD, skewness, kurtosis, entropy and homogeneity), second-order statistics based on GLCM (moments, ASM, IDM, contrast and entropy) and run length matrix in addition to wavelet features.

HISTOPATHOLOGIC ANALYSIS

All tissue samples were obtained through surgical resection or endoscopic biopsy, and each paraffin section containing tumor tissue was assessed by a dedicated pathologist. Genomic DNA was extracted from paraffin sections, and polymerase chain reaction and pyrosequencing were performed for KRAS (codons 12, 13 and 61). The sequence data generated with the ABI PRISM 3730 DNA analyzer (Applied Biosystems, Foster City, CA, USA) were analyzed using sequencing analysis software version 5.1.1 (Applied Biosystems).

STATISTICAL ANALYSIS

All statistical analyses were performed using MedCalc software for Windows (MedCalc Software version 12.7.1.0, Mariakerke, Belgium). A *p* value less than 0.05 was considered to be significant. To assess the association between the texture parameters and the presence of KRAS mutation, the Mann-Whitney U test was used. A receiver operating characteristic curve analysis was performed to evaluate the diagnostic performance of the texture parameters in predicting the presence of KRAS mutation, specifically by calculating the area under the curve (AUC). An optimal cut-off value for maximum accuracy was extracted, and additionally, the corresponding sensitivity, specificity, accuracy, positive predictive value (PPV) and negative predictive value (NPV) were estimated. The optimal cut-off value derived from the training dataset was verified using the validation dataset.

RESULTS

TRAINING DATASET

The training dataset consisted of a KRAS-mutant group ($n = 22$) and a wild-type group ($n = 24$). The histopathologic stages of the training dataset are shown in Table 2.

Skewness was significantly higher in the KRAS-mutant group than in the wild-type group (0.221 ± 0.283 ; -0.006 ± 0.178 , $p = 0.003$) (Figs. 1, 2). The AUC of skewness was 0.757 [95% confidence interval (CI), 0.606 to 0.872, $p = 0.0005$] (Fig. 3). When an optimal cut-off value of 0.078 was chosen, a maximum accuracy of 71% was achieved with a sensitivity of 64%, a specificity of 78%, a PPV of 74%, and a NPV of 69%. However, none of the other texture parameters showed any significant inter-group difference ($p > 0.05$). Table 3 summarizes the detailed results on the association between the texture parameters and KRAS mutation.

VALIDATION DATASET

The validation dataset consisted of a KRAS-mutant group ($n = 14$) and a wild-type group ($n = 19$). The AUC of skewness was 0.801 (95% CI, 0.625 to 0.919, $p = 0.0004$). When the cut-off value of 0.078 was applied to the validation dataset, skewness showed a sensitivity of 86%, a specific-

Table 2. Pathologic Stages of Training Dataset (pTN stage)

Stages	T1	T2	T3	T4	Total
N0	5	13	6	0	24
N1	0	5	5	1	11
N2	0	0	10	1	11
Total	5	18	21	2	46

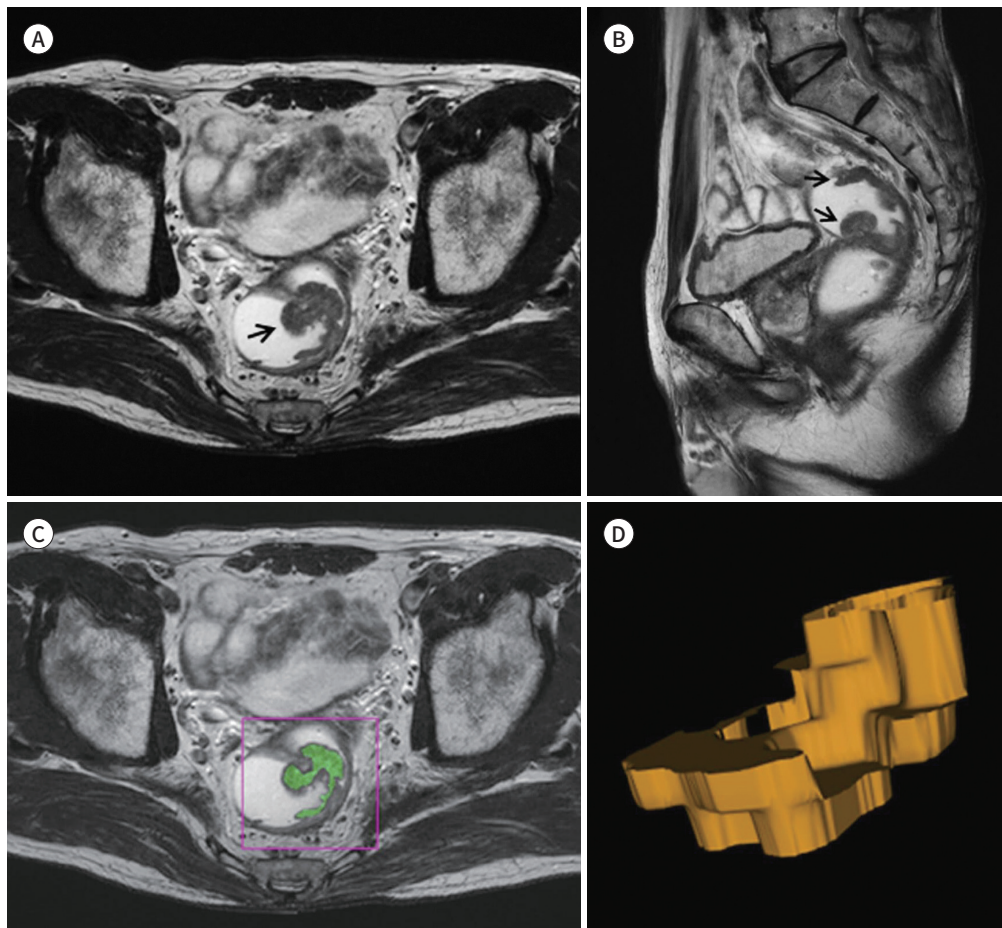
Fig. 1. A 70-year-old man with rectal adenocarcinoma and histopathology stage T2N0M0 with KRAS mutation.

A, B. T2-weighted axial (**A**) and sagittal (**B**) MR images show an ulcerofungating mass (arrows) in the mid-rectum.

C. Dedicated texture analysis software with 3D analysis automatically calculates the texture features of the ROI (green color), which was manually drawn along the tumor border on each slice of the axial T2WI.

D. 3D volume-rendered image of the whole tumor is obtained by automatic summation of multiple ROIs. The skewness of the whole tumor is 0.3665.

KRAS = Kirsten rat sarcoma viral oncogene homolog, ROI = region of interest, T2WI = T2-weighted turbo spin-echo, 3D = three-dimensional



ity of 68%, and an accuracy of 76%.

DISCUSSION

Our results revealed that among the texture parameters, skewness alone showed an association with KRAS-mutation status. Specifically, the KRAS-mutant group showed a higher value than did the wild-type group. In addition, skewness showed a moderate accuracy of 71% in differentiating the KRAS-mutant status, and internally validated as such. Skewness, as one of the first-order statistics in gray-level histogram features, represents the measure of asymmetry of the histogram distribution (3). As increased skewness reflects increased heterogeneity

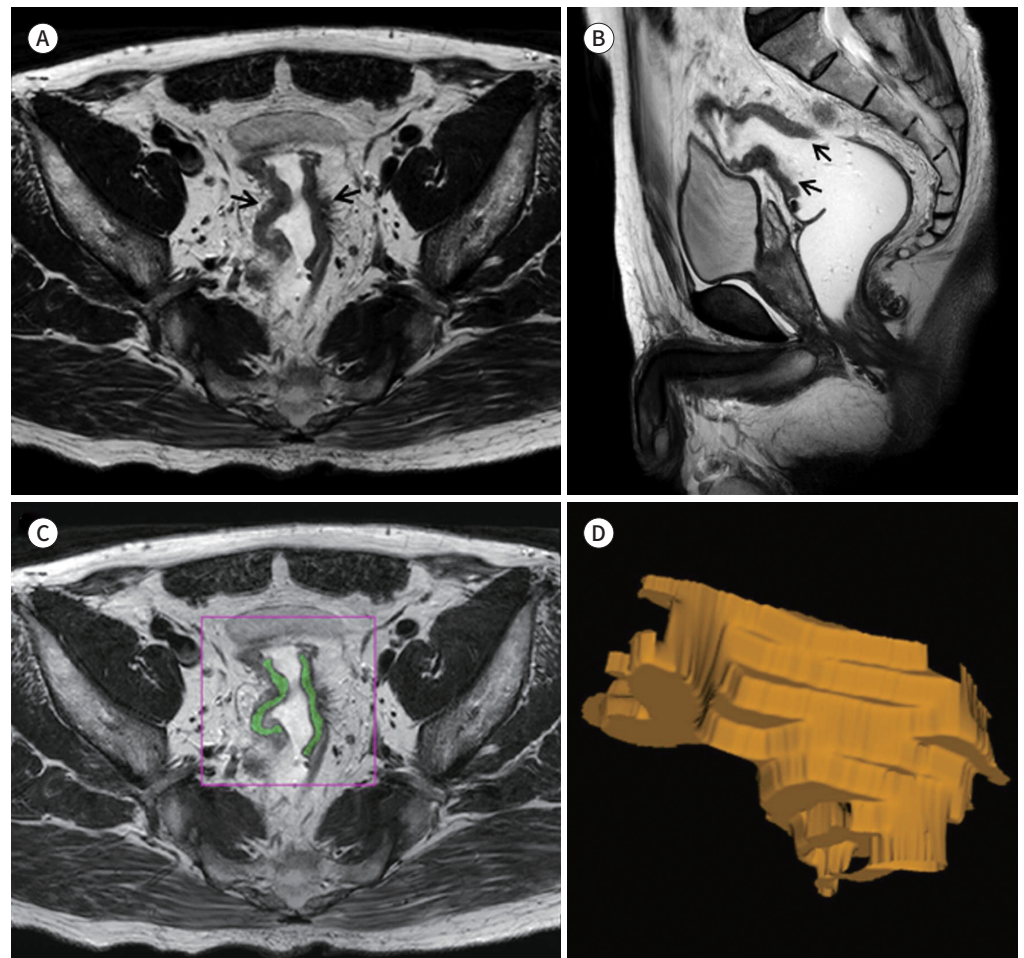
Fig. 2. A 57-year-old man with rectal adenocarcinoma and histopathology stage T3N1M0 without KRAS mutation.

A, B. T2-weighted axial (**A**) and sagittal (**B**) MR images show an ulceroinfiltrative mass (arrows) in the rectosigmoid junction.

C. Dedicated texture analysis software with 3D analysis automatically calculates the texture features of the ROI (green color), which was manually drawn along the tumor border on each slice of the axial T2WI.

D. 3D volume-rendered image of the entire tumor is obtained by automatic summation of multiple ROIs. The skewness of the whole tumor is -0.3003.

KRAS = Kirsten rat sarcoma viral oncogene homolog, ROI = region of interest, T2WI = T2-weighted turbo spin-echo, 3D = three-dimensional



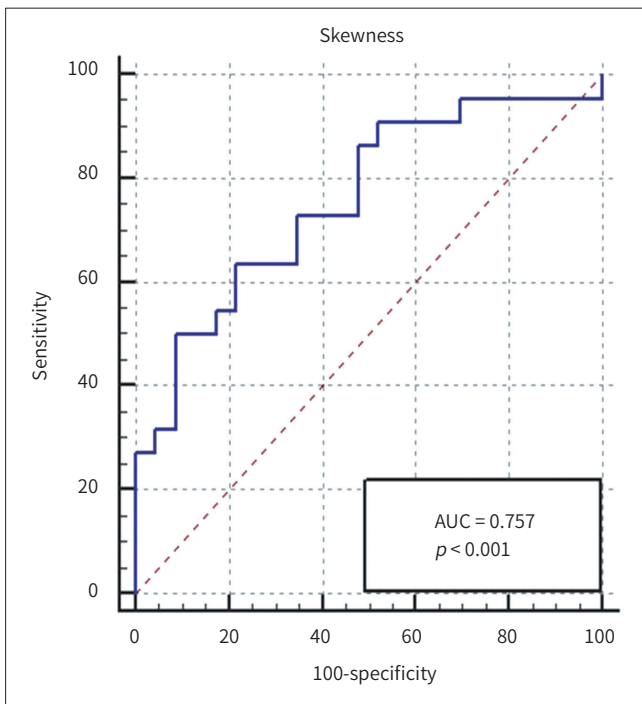


Fig. 3. ROC curve of the skewness for the prediction of KRAS mutation. The AUC is 0.757 (95% confidence interval, 0.606 to 0.872, $p = 0.0005$). When an optimal cut-off value of 0.078 is selected, the maximum accuracy of 71% is estimated with a sensitivity of 64% and a specificity of 78%. AUC = area under the curve, KRAS = Kirsten rat sarcoma viral oncogene homolog, ROC = receiver operating characteristic

in the signal intensity values in histogram, in our opinion, the KRAS-mutant group may have more heterogeneous tumor environment than the wild-type does.

Our results correspond well with a previous study (21). The investigators revealed that skewness with gradient filter based on T2WI showed higher values in the KRAS-mutant group than in the wild-type group and after incorporated into the decision tree with SDs, the diagnostic predictive values were a sensitivity of 84%, a specificity of 80% and an accuracy of 82% (21).

In addition to skewness with gradient filter, two Laplacian of Gaussian filtered features [SD for medium texture (spatial scale filter 3 and 4)] were found to be associated with KRAS-mutation status (21). In our opinion, tumor segmentation process may have accounted for the difference in the results. Whereas a single section with the largest tumor area was selected in the previous study, our study measured the entire tumor volume during tumor segmentation. In terms of the tumor heterogeneity, measurement on a single slice might have a great concern over the representative data and repeatability for tumor segmentation.

From the perspective of radiomics, a few other studies have investigated the association between radiomic signatures based on texture analysis and KRAS mutation (27, 28). Meng et al. (27) extracted radiomic signatures from multiparametric MRI including T2WI, T1-weighted images (T1WI), DWI, and dynamic contrast-enhanced (DCE) MRI, which showed an AUC of 0.651 (95% CI, 0.539 to 0.763) with an accuracy of 62%, a sensitivity of 58%, and a specificity of 64% in terms of KRAS mutation. Among the top 10 features used for acquisition of optimal radiomic signatures, 7 wavelet features were the majority. The authors found that the image features derived from each MRI sequence contributed to the optimal signature of KRAS mutation (3 on T1WI; 3 on DCE-MRI; 2 on T2WI; 2 on apparent diffusion coefficient map), and suggested that all MRI sequences are important and capable of providing comple-

mentary information in radiomics studies (27). However, T2WI is known to be an essential sequence for local staging. In our opinion, additional T1WI and DCE sequences are too much for routine protocol, therefore, they may be limitedly used for investigational purposes. Based on the previous diagnostic performance and ours which are superior to those on multi-parametric MRI as well as its labor-intensive work (21), we suggest that mono-parametric texture analysis on T2WI may be used for prediction of KRAS-mutation status and easily adapted to our daily practice.

There is no doubt that histopathology and molecular biologic test still play important roles in individualized treatment planning. However, patients have to undergo endoscopic or surgi-

Table 3. Association between Texture Parameters and KRAS Mutation

Texture Parameters	KRAS Mutant (n = 22)	Wild Type (n = 24)	p-Value
Histogram features			
Mean	216.856 ± 95.048	208.327 ± 79.314	0.9819
SD	30.303 ± 9.903	26.507 ± 9.357	0.1804
Skewness	0.221 ± 0.283	-0.006 ± 0.178	0.0030
Kurtosis	0.392 ± 0.669	0.091 ± 0.417	0.2469
Entropy	4.632 ± 0.293	4.502 ± 0.358	0.2963
Homogeneity	0.020 ± 0.022	0.023 ± 0.024	0.8737
GLCM-based features			
Moments	2.094 ± 0.744	2.543 ± 0.905	0.1021
ASM ($\times 10^{-3}$)	0.444 ± 0.252	0.550 ± 0.387	0.4268
IDM	0.121 ± 0.043	0.131 ± 0.048	0.5102
Contrast ($\times 10^3$)	3.068 ± 5.668	1.366 ± 1.421	0.2469
Entropy	3.668 ± 0.249	3.600 ± 0.268	0.4008
GLRLM-based features			
Energy ($\times 10^8$)	9.227 ± 10.401	6.101 ± 6.262	0.340
Compactness 1	9.729 ± 4.832	8.027 ± 3.446	0.286
Compactness 2	0.148 ± 0.213	0.242 ± 0.808	0.180
GLN	186.428 ± 263.209	123.999 ± 125.253	0.555
Wavelet features*			
Wavelet HHH	0.038 ± 1.343	0.407 ± 0.757	0.6662
Wavelet HHL	0.969 ± 2.294	0.412 ± 0.919	0.4815
Wavelet HLH	0.952 ± 2.284	0.395 ± 0.921	0.4401
Wavelet HLL	7.980 ± 8.620	4.625 ± 3.132	0.3289
Wavelet LHH	0.925 ± 2.278	0.382 ± 0.922	0.4537
Wavelet LHL	7.910 ± 8.632	4.522 ± 3.091	0.3403
Wavelet LLH	7.879 ± 8.675	4.442 ± 3.077	0.3289
Wavelet LLL	159.540 ± 73.680	165.640 ± 79.340	0.7334

Data are mean ± SD.

*Three-dimensional wavelet transformation was applied and filtered with low-pass filter (L) or high-pass filter (H) along x, y, and z axes, respectively.

ASM = angular second moment, GLCM = gray-level co-occurrence matrix, GLN = gray-level non-uniformity, GLRLM = gray-level run-length matrix, IDM = inverse difference moment, KRAS = Kirsten rat sarcoma viral oncogene homolog, SD = standard deviation

cal resection at the expense of invasive tissue sampling and potential risk of complications such as bleeding. From a radiological perspective, patients benefit from preoperative MRI by obtaining KRAS mutation status with the non-invasive imaging modality at no additional cost.

This study has several limitations. First, the current study was an explorative feasibility study, thus the retrospective study design and relatively small study population of the validation dataset could be considered. Further studies with large cohorts are warranted. Second, we focused only on the association between texture features and KRAS-mutation status. However, CRC is associated with multiple biological and genetic characteristics (29), and thus, studies on radiogenomics are necessary in order to comprehensively evaluate multiple biological and genetic characteristics. Third, texture features can be affected by many factors, such as field strength, sequences, and imaging parameters, which are related to MRI signal intensity as well as imaging modality difference (27). Therefore, we tried to make a uniform environment with the same 3T-MR machine, sequence and imaging parameters.

In conclusion, skewness derived from texture analysis based on T2WI was associated with KRAS mutation in patients with non-mucinous rectal cancer.

Author Contributions

Conceptualization, K.S.H.; data curation, K.S.H., J.S.J.; formal analysis, K.S.H., J.S.J.; funding acquisition, K.S.H.; investigation, K.S.H., J.S.J.; methodology, K.S.H., J.S.J.; project administration, K.S.H.; resources, all authors; software, P.S.J.; supervision, K.S.H.; validation, all authors; visualization, K.S.H., J.S.J.; writing—original draft, all authors; and writing—review & editing, all authors.

Conflicts of Interest

The authors have no potential conflicts of interest to disclose.

Funding

This work was supported by the 2019 Inje University research grant.

REFERENCES

1. Srinivasan GN, Shobha G. Statistical texture analysis. *Proc World Acad Sci Eng Technol* 2008;36:1264-1269
2. Materka A. Texture analysis methodologies for magnetic resonance imaging. *Dialogues Clin Neurosci* 2004;6:243-250
3. Duvauferrier R, Bezy J, Bertaud V, Toussaint G, Morelli J, Lasbleiz J. Texture analysis software: integration with a radiological workstation. *Stud Health Technol Inform* 2012;180:1030-1034
4. Davnall F, Yip CS, Ljungqvist G, Selmi M, Ng F, Sanghera B, et al. Assessment of tumor heterogeneity: an emerging imaging tool for clinical practice? *Insights Imaging* 2012;3:573-589
5. Gadkari D. Image quality analysis using GLCM [dissertation]. Orlando: University of Central Florida 2004
6. De Cecco CN, Ganeshan B, Ciolina M, Rengo M, Meinel FG, Musio D, et al. Texture analysis as imaging biomarker of tumoral response to neoadjuvant chemoradiotherapy in rectal cancer patients studied with 3-T magnetic resonance. *Invest Radiol* 2015;50:239-245
7. Jalil O, Afaq A, Ganeshan B, Patel UB, Boone D, Endozo R, et al. Magnetic resonance based texture parameters as potential imaging biomarkers for predicting long-term survival in locally advanced rectal cancer treated by chemoradiotherapy. *Colorectal Dis* 2017;19:349-362
8. Liu L, Liu Y, Xu L, Li Z, Lv H, Dong N, et al. Application of texture analysis based on apparent diffusion coefficient maps in discriminating different stages of rectal cancer. *J Magn Reson Imaging* 2017;45:1798-1808
9. Horvat N, Veeraraghavan H, Khan M, Blazic I, Zheng J, Capanu M, et al. MR imaging of rectal cancer: radiomics analysis to assess treatment response after neoadjuvant therapy. *Radiology* 2018;287:833-843
10. Cui Y, Yang X, Shi Z, Yang Z, Du X, Zhao Z, et al. Radiomics analysis of multiparametric MRI for prediction of pathological complete response to neoadjuvant chemoradiotherapy in locally advanced rectal cancer. *Eur*

Radiol 2019;29:1211-1220

11. Liu Z, Zhang XY, Shi YJ, Wang L, Zhu HT, Tang Z, et al. Radiomics analysis for evaluation of pathological complete response to neoadjuvant chemoradiotherapy in locally advanced rectal cancer. *Clin Cancer Res* 2017;23:7253-7262
12. Nie K, Shi L, Chen Q, Hu X, Jabbour SK, Yue N, et al. Rectal cancer: assessment of neoadjuvant chemoradiation outcome based on radiomics of multiparametric MRI. *Clin Cancer Res* 2016;22:5256-5264
13. Liu H, Zhang C, Wang L, Luo R, Li J, Zheng H, et al. MRI radiomics analysis for predicting preoperative synchronous distant metastasis in patients with rectal cancer. *Eur Radiol* 2019;29:4418-4426
14. Chen LD, Liang JY, Wu H, Wang Z, Li SR, Li W, et al. Multiparametric radiomics improve prediction of lymph node metastasis of rectal cancer compared with conventional radiomics. *Life Sci* 2018;208:55-63
15. Sun Y, Hu P, Wang J, Shen L, Xia F, Qing G, et al. Radiomic features of pretreatment MRI could identify T stage in patients with rectal cancer: preliminary findings. *J Magn Reson Imaging* 2018;48:615-621
16. Newton KF, Newman W, Hill J. Review of biomarkers in colorectal cancer. *Colorectal Dis* 2012;14:3-17
17. Andreyev HJ, Norman AR, Cunningham D, Oates JR, Clarke PA. Kirsten ras mutations in patients with colorectal cancer: the multicenter "RASCAL" study. *J Natl Cancer Inst* 1998;90:675-684
18. Andreyev HJ, Norman AR, Cunningham D, Oates J, Dix BR, Iacopetta BJ, et al. Kirsten ras mutations in patients with colorectal cancer: the 'RASCAL II' study. *Br J Cancer* 2001;85:692-696
19. Taylor FG, Swift RI, Blomqvist L, Brown G. A systematic approach to the interpretation of preoperative staging MRI for rectal cancer. *AJR Am J Roentgenol* 2008;191:1827-1835
20. Nougaret S, Reinhold C, Mikhael HW, Rouanet P, Bibeau F, Brown G. The use of MR imaging in treatment planning for patients with rectal carcinoma: have you checked the "DISTANCE"? *Radiology* 2013;268:330-344
21. Oh JE, Kim MJ, Lee J, Hur BY, Kim B, Kim DY, et al. Magnetic resonance-based texture analysis differentiating KRAS mutation status in rectal cancer. *Cancer Res Treat* 2020;52:51-59
22. Choi TW, Kim JH, Park SJ, Ahn SJ, Joo I, Han JK. Risk stratification of gallbladder polyps larger than 10 mm using high-resolution ultrasonography and texture analysis. *Eur Radiol* 2018;28:196-205
23. Park HJ, Kim JH, Choi SY, Lee ES, Park SJ, Byun JY, et al. Prediction of therapeutic response of hepatocellular carcinoma to transcatheter arterial chemoembolization based on pretherapeutic dynamic CT and textural findings. *AJR Am J Roentgenol* 2017;209:W211-W220
24. Choi TW, Kim JH, Yu MH, Park SJ, Han JK. Pancreatic neuroendocrine tumor: prediction of the tumor grade using CT findings and computerized texture analysis. *Acta Radiol* 2018;59:383-392
25. Ahn SJ, Kim JH, Park SJ, Han JK. Prediction of the therapeutic response after FOLFOX and FOLFIRI treatment for patients with liver metastasis from colorectal cancer using computerized CT texture analysis. *Eur J Radiol* 2016;85:1867-1874
26. Ryu YJ, Choi SH, Park SJ, Yun TJ, Kim JH, Sohn CH. Glioma: application of whole-tumor texture analysis of diffusion-weighted imaging for the evaluation of tumor heterogeneity. *PLoS One* 2014;9:e108335
27. Meng X, Xia W, Xie P, Zhang R, Li W, Wang M, et al. Preoperative radiomic signature based on multiparametric magnetic resonance imaging for noninvasive evaluation of biological characteristics in rectal cancer. *Eur Radiol* 2019;29:3200-3209
28. Yang L, Dong D, Fang M, Zhu Y, Zang Y, Liu Z, et al. Can CT-based radiomics signature predict KRAS/NRAS/BRAF mutations in colorectal cancer? *Eur Radiol* 2018;28:2058-2067
29. Arvelo F, Sojo F, Cotte C. Biology of colorectal cancer. *Ecancermedicalscience* 2015;9:520

원발성 비점액성 직장암 환자에서 자기공명영상 기반 텍스처 분석 변수와 KRAS 유전자 변이와의 연관성

조성재¹ · 김승호^{1*} · 박상준² · 이예다운¹ · 손정희¹

목적 원발성 비점액성 직장암 환자에서 자기공명영상 기반 텍스처 분석 변수와 Kirsten rat sarcoma viral oncogene homolog (이하 KRAS) 유전자 변이와의 연관성을 조사한다.

방법 조직학적으로 비점액성 직장 선암종으로 진단받고 KRAS 유전자 정보가 있으며 치료 전 직장 자기공명영상을 시행한 79명의 환자를 훈련 데이터셋($n = 46$)과 검증 데이터셋($n = 33$)으로 나누었다. 텍스처 분석은 축상면 T2 강조영상에서 시행되었다. 텍스처 변수와 KRAS 유전자 변이와의 연관성은 Mann-Whitney U 검정을 통해 통계적으로 분석하였다. 수신기작동 특성 곡선(receiver operating characteristic) 분석을 이용하여 KRAS 유전자 변이를 예측하기 위한 최적의 절단값을 산출하였다. 이 절단값은 검증 데이터셋을 사용해 검증되었다.

결과 훈련 데이터셋에서 왜도(skewness)는 유전자 변이가 있는 집단($n = 22$ 명)에서 유전자 변이가 없는 집단($n = 24$ 명)보다 유의하게 높았다(0.221 ± 0.283 ; -0.006 ± 0.178 , $p = 0.003$). 왜도의 곡선 하 면적 값(area under the curve)은 0.757 (95% 신뢰구간, 0.606–0.872)로 정확도는 71%, 민감도는 64%, 특이도는 78%였다. 다른 텍스처 변수들은 두 집단 간 유의한 차이를 보이지 않았다($p > 0.05$). 검증 데이터셋에 절단값 0.078을 적용하였을 때 정확도는 76%, 민감도는 86%, 특이도는 68%였다.

결론 원발성 비점액성 직장암 환자에서 왜도는 KRAS 유전자 변이와 연관성을 보였다.

¹인제대학교 의과대학 해운대백병원 영상의학과,

²서울대학교병원 영상의학과